Published in IET Power Electronics
Received on 29th January 2014
Revised on 16th April 2014
Accepted on 15th June 2014
doi: 10.1049/iet-pel.2014.0061

ISSN 1755-4535

Novel grid voltage estimation by means of the Newton–Raphson optimisation for three-phase grid connected voltage source converters

Hosein Gholami-Khesht, Mohammad Monfared

Department of Electrical Engineering, Faculty of Engineering, Ferdowsi University of Mashhad, Mashhad, Iran
E-mail: m.monfared@um.ac.ir

Abstract: This study presents a proportional resonant current control scheme for three-phase grid connected voltage source converters without any grid voltage sensors. Towards this goal, the grid voltage sensors are replaced by a voltage estimation scheme based on the Newton–Raphson algorithm. In the proposed method, the grid connected converter behaviour is converted to an optimisation problem which relates the instantaneous grid voltage value to the filter parameters, the generated converter voltage and the exchanged powers in each sampling period. The proposed optimisation problem is then solved in each sampling period by means of the Newton–Raphson optimisation technique. Afterwards, the reference current for the current control loop is generated from the estimated grid voltages. Using an estimator instead of the voltage sensors not only reduces the size and cost of the converter system but also improves its reliability and protects it from grid voltage disturbances and noises. The excellent performance of the proposed grid voltage sensorless scheme is confirmed through experimental and simulation results.

1 Introduction

Recently, three-phase pulse-width modulated (PWM) voltage source converters (VSCs) have found widespread applications in grid connected energy systems, such as renewables (wind turbines and photovoltaics) [1, 2], micro grids [3], flexible AC transmission systems [4], active power filters [5], high-voltage direct current [1] and uninterruptible power supplies [6]. The most important features of the VSCs are the ability to use advanced modulation techniques, bi-directional and independent control of active and reactive powers, adjustable input and output power factor and fast and accurate current regulation with low total harmonic distortion (THD). To extract the maximum benefit from the VSCs, various control strategies are available now [7–31]. Generally, almost all of these methods require three kinds of sensors in their structure: (i) DC-link voltage sensor; (ii) line current sensors; and (iii) line voltage sensors. In an aim to reduce the cost and size of grid connected converters and also improve the reliability, many efforts have been done on control schemes that eliminate some of these sensors from the converter system, offering some kind of sensorless operation [7–24].

The DC-link voltage sensor and the line current sensors are required for both control and protection purposes, so owning to their vital role in over voltage and over current protection, they cannot be omitted without risk of harm for personnel or equipment. Meanwhile, the grid voltage information is only used in the control system, mainly for synchronising the VSC with the grid. Therefore the grid voltage sensors can be safely replaced with a software algorithm which uses the converter parameters and other measured quantities as its inputs to estimate the instantaneous value of the AC voltage.

The most convenient voltage estimation method consists of adding the converter output voltage to the voltage drop on the AC filter, which in most applications is a single inductance. Despite its simplicity, it requires the numerical differentiation of the sampled converter current which is very sensitive to noise and can be concluded as a serious drawback for this method. Furthermore, the neutral point variations of the converter must be considered in the calculations [8, 9].

In voltage estimations based on instantaneous powers [9, 10], firstly instantaneous active and reactive powers are estimated using the measured currents, the measured DC-link voltage, the switching state and the filter inductance. Afterwards, grid voltages are calculated from the estimated powers and measured currents. Similar to the pervious method, high-frequency noises owning to the differentiation operation are amplified. Therefore to achieve a good estimation performance a high sampling frequency and a large inductance are required.

Furthermore, the estimation accuracy is highly deteriorated, or even impossible, under light load conditions (near zero currents), because the estimated voltage is obtained from division of the estimated power by the amplitude of the measured current.

Virtual flux (VF) is one of the most commonly used concepts in applications of grid connected VSCs [11–14]. It not only does not require any differentiation or division in

its structure, but also because of the intrinsic integration existed in the algorithm, the effect of distorted grid voltage on the control system is reduced. However, practical implementation of a perfect VF estimator is based on an ideal integrator and is not possible. Noises and the DC offset in the measured currents cause drift and saturation. To overcome these problems, solutions such as low-pass filtering [11, 12], band-pass filtering [13] and frequency-adaptive band-pass filtering [14] are proposed. The steady-state error in estimated voltages, sensitivity to frequency variations, complicated structure and necessity of a FLL are considered as main shortcomings associated to these methods.

Adaptive observers like Kalman filters [15, 16], Luenberger observers [17] and other mathematical optimisations [18–21] could attract many attentions in recent years. These methods are used to estimate unknown parameters and states by minimising the error between the actual (measured) states and the predicted states. Good dynamic and accuracy are some of their advantages and complexity of estimation algorithm, difficulty of tuning the observer gain (which is a trade-of between the system stability and the convergence speed) and high computational burden are recognised as their serious disadvantages.

Voltage sensorless control methods based on the one-cycle control are proposed in [22–24], which have the benefits of simple structure, and fast dynamic response because of continuous corrective action of analogue implementation. However, these techniques suffer from some serious drawbacks, such as controller modification is not possible without hardware re-design because of analogue implementation, the assumption that the grid voltage amplitude is known and constant, the limited operation to the unity power factor and poor performance under light load conditions and when the converter is operating in the inverting mode.

In this paper, a proportional resonant (PR) based current control without any AC side voltage sensor for the grid connected VSC is presented. In the proposed method, the grid voltage is estimated using the converter system equations that relate the converter voltage, the grid voltage, and the exchanged power between the grid and the VSC in the time domain. These equations are non-linear and the Newton–Raphson optimisation algorithm is employed to solve the non-linear equations in each sampling period.

Newton–Raphson algorithm is the most widely utilised method in power system applications because of its fast convergence characteristic in offline solving of non-linear mathematical problems, such as power flow equations. Considerable improvements in signal processors in recent years have led to use of this powerful mathematical tool for solving various online optimisation problems [25].

The rest of paper is organised as follows. Details of the proposed grid voltage sensorless technique will be presented in Section 2. Section 3 presents the practical implementation considerations of the proposed grid voltage estimation method, and finally, the proper operation of the proposed scheme is confirmed through extensive simulations and experimental tests in Section 4.

2 Proposed control scheme

Fig. 1 shows the single-line representation of the power circuit in presence of the proposed control scheme, which comprises the reference current generator from the reference powers and the estimated grid voltage, the grid voltage estimator from the converter reference voltage and the grid current and the current control loop, where the symbols are defined as follows:

v_S, i grid voltage and current
v converter AC-side output voltage
V_{dc} DC-link voltage

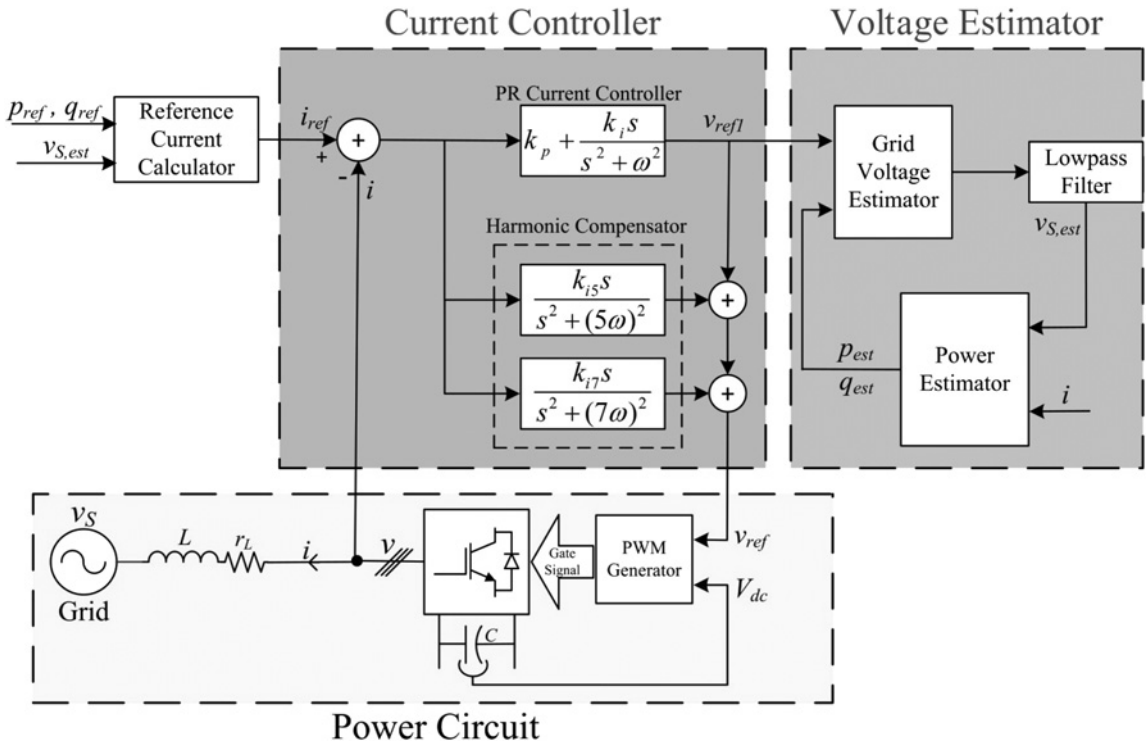

Fig. 1 *Proposed control scheme for the grid connected VSC*

doi: 10.1049/iet-pel.2014.0061

L, r_L filter inductance and equivalent series resistance
$v_{S,\text{est}}$ estimated grid voltage
p_{ref}, q_{ref} active and reactive powers references
p_{est}, q_{est} estimated active and reactive powers (injected into grid)
i_{ref} current reference
v_{ref} converter reference voltage
v_{ref1} output of the PR controller

The current control loop uses PR controllers and selective harmonic compensators (SHCs) in the stationary reference frame to regulate the grid current and further attenuate the low-order harmonic components, respectively [1, 2, 26–29].

As it can be seen, the SHC network includes resonators at the desired harmonic frequencies to be attenuated (here fifth and seventh).

At the first stage of the block diagram of Fig. 1, the reference converter currents for the PR regulators are generated from the estimated grid voltages and the reference powers, in accordance with the following equation

$$\begin{bmatrix} i_{\alpha,\text{ref}} \\ i_{\beta,\text{ref}} \end{bmatrix} = \frac{1}{\left(v_{S\alpha,\text{est}}{}^2 + v_{S\beta,\text{est}}{}^2\right)} \begin{bmatrix} v_{S\alpha,\text{est}} & v_{S\beta,\text{est}} \\ v_{S\beta,\text{est}} & -v_{S\alpha,\text{est}} \end{bmatrix} \begin{bmatrix} p_{\text{ref}} \\ q_{\text{ref}} \end{bmatrix} \tag{1}$$

In (1), $i_{\alpha,\text{ref}}$ and $i_{\beta,\text{ref}}$ are the converter reference currents, and $v_{S\alpha,\text{est}}$ and $v_{S\beta,\text{est}}$ are the estimated grid voltages in the stationary ($\alpha\beta$) reference frame.

Grid voltages are estimated in each sampling period from the converter system equations with the Newton–Raphson iterative algorithm. The following subsection demonstrates how the converter equations are derived and the Newton–Raphson is adopted to our specific problem.

2.1 Calculation of exchanged power between VSC and power grid

Fig. 2 depicts the power stage of the grid connected three-phase VSC. Based on this figure, the injected active and reactive power into the grid can be written as shown in (2)

$$S = p + \text{j}q = V_S \times \left(\frac{V\angle\delta - V_S}{r_L + \text{j}X}\right)^* \tag{2}$$

where p and q are active and reactive powers, X and r_L are the reactance and resistance of the filter inductor, V_S and V are the amplitude of grid and converter voltage, respectively, and δ is the power angle (phase-angle difference between the converter and grid voltages). Equation (2) can be rewritten as

$$\begin{cases} p = \dfrac{V_S}{r_L^2 + X^2}\left[r_L V\cos(\delta) - r_L V_S + XV\sin(\delta)\right] \\ q = \dfrac{V_S}{r_L^2 + X^2}\left[-r_L V\sin(\delta) - XV_S + XV\cos(\delta)\right] \end{cases} \tag{3}$$

As seen in (3), both expressions are complicated and depend highly on the filter impedance. To overcome these problems, the concept of virtual power that is introduced in [30, 31] is adopted here. Hence, p and q are transformed into virtual

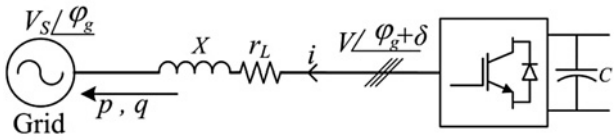

Fig. 2 *Single-line representation of the grid connected VSC*

powers p' and q' through the following linear transformations

$$\begin{cases} p' = Xp - r_L q \\ q' = r_L p + Xq \end{cases} \tag{4}$$

Substituting (3) into (4) yields

$$\begin{cases} p' = V_S V\sin(\delta) \\ q' = V_S[V\cos(\delta) - V_S] \end{cases} \tag{5}$$

The above expressions for virtual active and reactive powers are much more simple than (3), and are independent from the reactance and the resistance of the filter.

2.2 Proposed voltage estimation algorithm

Assuming that p', q' and V are known, V_S and δ can be calculated in each sampling period from (5). After calculating δ, phase-angle of the grid voltage (φ_g) is simply obtained from the phase-angle of the converter voltage ($\varphi_c = \varphi_g + \delta$) which is already known as

$$\varphi_g = \varphi_c - \delta \tag{6}$$

As mentioned before, φ_c is the phase-angle of the converter voltage which can be easily calculated from the reference converter voltages as shown in (7).

$$\varphi_c = \arctan\left(\frac{V_{\beta,\text{ref}}}{V_{\alpha,\text{ref}}}\right) \tag{7}$$

In summary, to evaluate the instantaneous grid voltage in each sampling period, one can solve, by any means, (5) for V_S and δ (and consequently φ_g). Now, components of the grid voltage in the stationary reference frame can be readily calculated as

$$\begin{cases} v_{S\alpha,\text{est}} = V_S\sin(\varphi_g) \\ v_{S\beta,\text{est}} = -V_S\cos(\varphi_g) \end{cases} \tag{8}$$

2.3 Numerical solution based on the Newton–Raphson method

Assuming that V_S and δ must be evaluated, (5) is apparently a system of two non-linear interconnected equations which is complicated enough to preclude an analytical solution; instead, numerical techniques must be used, which is the topic of this subsection.

In this paper, (5) is solved with acceptable accuracy and reasonable effort based on the Newton–Raphson iterative method, the principles of which will now be explained.

To formulate the Newton–Raphson optimisation problem in terms of the unknowns V_S and δ, the system of (5) can

be rewritten as

$$\begin{cases} f(\delta, V_S) = p' - VV_S \sin(\delta) = 0 \\ g(\delta, V_S) = q' - V_S[V\cos(\delta) - V_S] = 0 \end{cases} \quad (9)$$

In (9), $f(\delta, V_S)$ and $g(\delta, V_S)$ are the mismatches between the real and calculated virtual active and reactive powers, respectively. To evaluate (9), p' and q' can be computed using the estimated voltages and measured currents, in accordance to (10), or simply be replaced by the reference values for the powers (p_{ref}, q_{ref}) which must be first transformed into virtual references through (4)

$$\begin{pmatrix} p' \\ q' \end{pmatrix} = \begin{pmatrix} p'_{\text{est}}(k) \\ q'_{\text{est}}(k) \end{pmatrix} = \begin{pmatrix} X & -r_L \\ r_L & X \end{pmatrix} \begin{pmatrix} v_{S\alpha,\text{est}}(k) & v_{S\beta,\text{est}}(k) \\ v_{S\beta,\text{est}}(k) & -v_{S\alpha,\text{est}}(k) \end{pmatrix} \begin{pmatrix} i_\alpha(k) \\ i_\beta(k) \end{pmatrix} \quad (10)$$

The Jacobian matrix ($\boldsymbol{J}_{\text{est}}$) for (9) is formed as

$$J_{\text{est}} = \begin{bmatrix} \frac{\partial f}{\partial \delta} & \frac{\partial f}{\partial V_S} \\ \frac{\partial g}{\partial \delta} & \frac{\partial g}{\partial V_S} \end{bmatrix} \quad (11)$$

where

$$\begin{cases} \frac{\partial f}{\partial \delta} = V_S V\cos(\delta) \\ \frac{\partial f}{\partial V_S} = V\sin(\delta) \\ \frac{\partial g}{\partial \delta} = -V_S V\sin(\delta) \\ \frac{\partial g}{\partial V_S} = V\cos(\delta) - 2V_S \end{cases} \quad (12)$$

Given initial values V_{S0} and δ_0, the iterations of the Newton–Raphson algorithm are performed through evaluating the following equations

$$\begin{bmatrix} \Delta\delta_k \\ \Delta V_{S,k} \end{bmatrix} = J^{-1}_{\text{est},k} \begin{bmatrix} f(\delta_k, V_{S,k}) \\ g(\delta_k, V_{S,k}) \end{bmatrix} \quad (13)$$

$$\begin{cases} \delta_{k+1} = \delta_k + \Delta\delta_k \\ V_{S,k+1} = V_{S,k} + \Delta V_{S,k} \end{cases} \quad (14)$$

Iterations are terminated once the values of $f(\delta, V_S)$ and $g(\delta, V_S)$ are small enough. It should be mentioned that while the optimisation is solved in each sampling period, but once V_S and δ are updated successfully, they will not experience a considerable change until the system conditions (grid voltages or exchanged powers) change remarkably.

In engineering problems the Newton–Raphson method has proved most successful thanks to its fast and strong convergence characteristics. However, if a given problem has saddles or multiple roots, the algorithm may get trapped in a suboptimal solution or even become unstable. Therefore it is very important that the convergence condition of the algorithm is investigated, before it is implemented. Equation (12) show that all four elements of the Jacobian matrix are monotonous and do not have saddles or multiple roots. Therefore this problem will always convergence to the right solution and will yield to a close approximation of δ and V_S.

In most practical conditions, the power angle (δ) is small. Hence, it can be safely assumed that $\sin(\delta) = 0$ and $\cos(\delta) = 1$. Considering these assumptions, the Jacobian matrix will be simplified to

$$J_{\text{est}} = \begin{bmatrix} V_S V & 0 \\ 0 & V - 2V_S \end{bmatrix} \quad (15)$$

Eventually, by substituting (9) and (15) in (13), the iterations of the Newton–Raphson algorithm are conducted through evaluating the following simple equations

$$\begin{cases} \Delta\delta_k = \frac{p_k{}'}{VV_{S,k}} - \sin(\delta_k) \\ \Delta V_{S,k} = \left(\frac{1}{V - 2V_{S,k}}\right)(q_k{}' - V_{S,k}(V\cos(\delta_k) - V_{S,k})) \end{cases} \quad (16)$$

3 Practical considerations

In this section, some practical aspects are investigated. The proper solution for the converter voltage acquisition being first discussed, a suggestion for compensation of the control and estimation delay follows. This is continued by a discussion of the startup process of the controller.

3.1 Converter voltage acquisition

As mentioned before, the grid voltage estimation algorithm needs the converter developed voltage as one of its inputs. The converter output voltage can be obtained with three different methods: (i) direct monitoring that needs additional measurements; (ii) reconstructing the converter voltage by using the DC-link voltage and the switching states [9]; and (iii) using the converter reference voltage instead, which is the input to the PWM modulator [11]. First and second methods are heavily polluted with switching noises and require some kind of filtering. In a PWM-VSC, it is possible to use the converter reference voltage instead of the actual converter voltage. This technique is simple and noise-resistant. Although, when the reference voltage is used, some error compensation schemes must also be used to obtain high accuracy, such as voltage limitation and PWM delay compensation.

Table 1 System parameters

Power circuit	
phase grid voltage	42 (60) Vrms (Peak)
DC-link voltage	140 V
filter inductance	2 mH
filter resistance	0.6 Ω
grid frequency	50 Hz
sampling and switching frequency	5 kHz
Control system	
k_p (PR controller)	4
k_i (PR controller)	5000
k_{i5} and k_{i7} (harmonic compensator)	5000
discretisation method	tustin
cutoff frequency (second-order LPF)	700 Hz
damping factor (second-order LPF)	0.707

doi: 10.1049/iet-pel.2014.0061

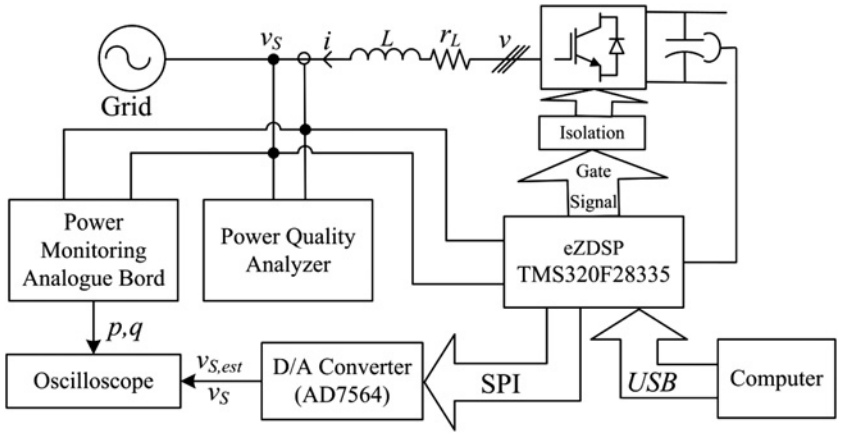

Fig. 3 *Schematic diagram of the experimental test bench*

3.2 Delay compensation

In practice, there always exists a time delay between the actual grid voltage and the estimated grid voltage because of delays introduced by the analogue to digital converters (ADCs), the program execution, and the PWM modulator. In most applications it can be assumed that the grid voltage is estimated with one sampling period time delay. This delay causes a small error in the injected active and reactive powers. In order to compensate for this delay, the phase of the estimated grid voltage is leaded with a sampling period as shown in (17)

$$\begin{cases} v'_{S\alpha\beta,\text{est}} = v_{S\alpha\beta,\text{est}} \exp(\text{j}\Delta\theta) \\ \Delta\theta = T_s\omega \end{cases} \tag{17}$$

where, $v_{S\alpha\beta,\text{est}}$, $v'_{S\alpha\beta,\text{est}}$ and T_s are the estimated voltage, leaded (compensated) estimated voltage and the sampling period, respectively. Equation (17) can be rewritten as

$$\begin{cases} v'_{S\alpha,\text{est}} = v_{S\alpha,\text{est}} \cos(\Delta\theta) - v_{S\beta,\text{est}} \sin(\Delta\theta) \\ v'_{S\beta,\text{est}} = v_{S\beta,\text{est}} \cos(\Delta\theta) + v_{S\alpha,\text{est}} \sin(\Delta\theta) \end{cases} \tag{18}$$

In order to save time in calculating (18), the trigonometric functions can be precalculated, because $\Delta\theta$ is already known.

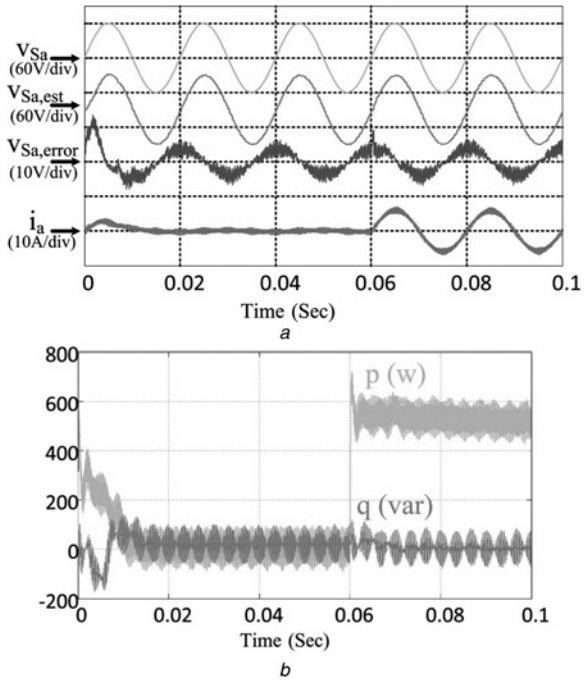

Fig. 4 *Simulated startup performance of the proposed method*

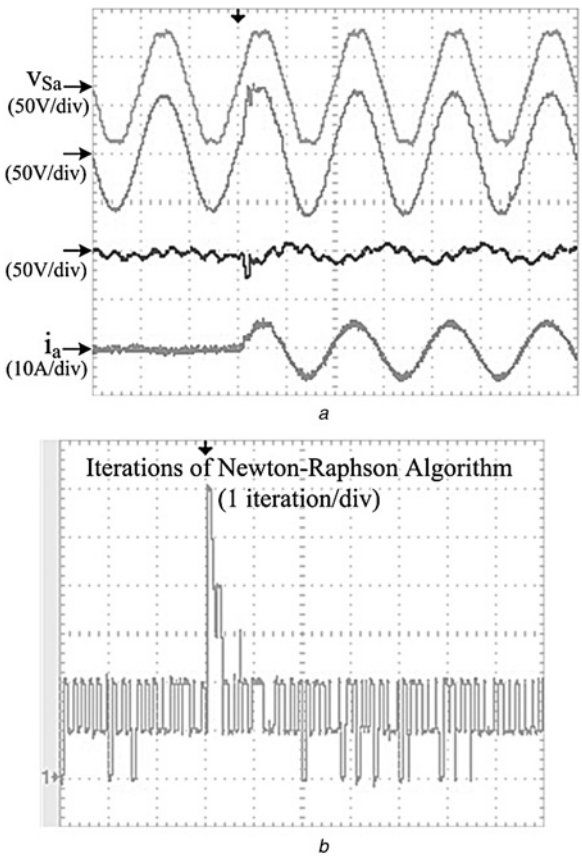

Fig. 5 *Experimental startup performance of the proposed method*

a Startup waveforms
b Iterations of the Newton–Raphson algorithm

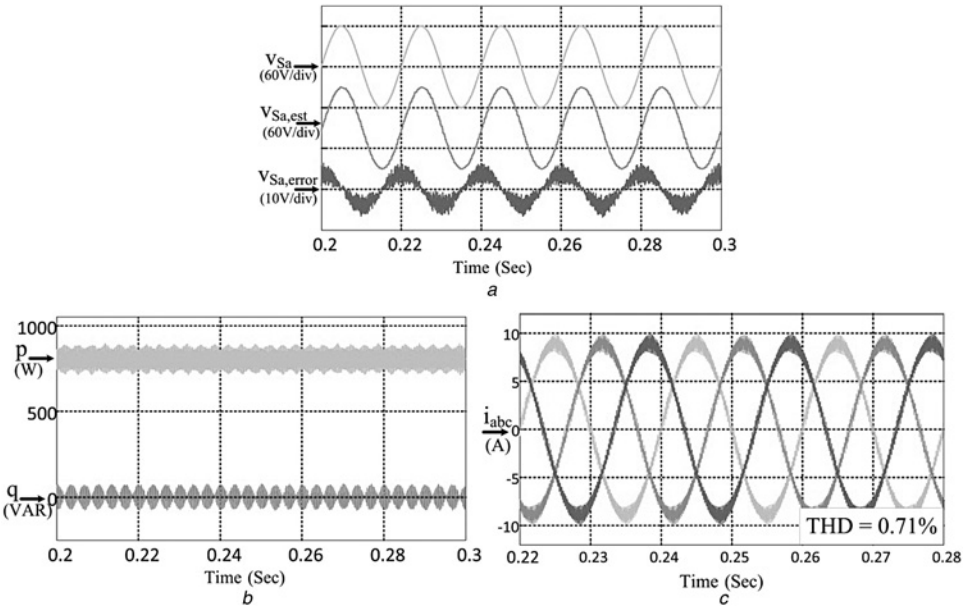

Fig. 6 *Simulated steady-state performance of the proposed grid voltage sensorless method*

a Grid voltage and its estimation
b Exchanged powers
c Three-phase grid currents

3.3 Startup process

It is clear that the proper selection of initial values speeds-up the Newton–Raphson process. In our problem, it is convenient to select the initial guesses as the nominal grid voltage value for V_S and zero for δ.

4 Performance evaluations

To verify the feasibility and effectiveness of the proposed sensorless control scheme, several simulation and experimental tests have been designed under various operation conditions. The simulation and experimental

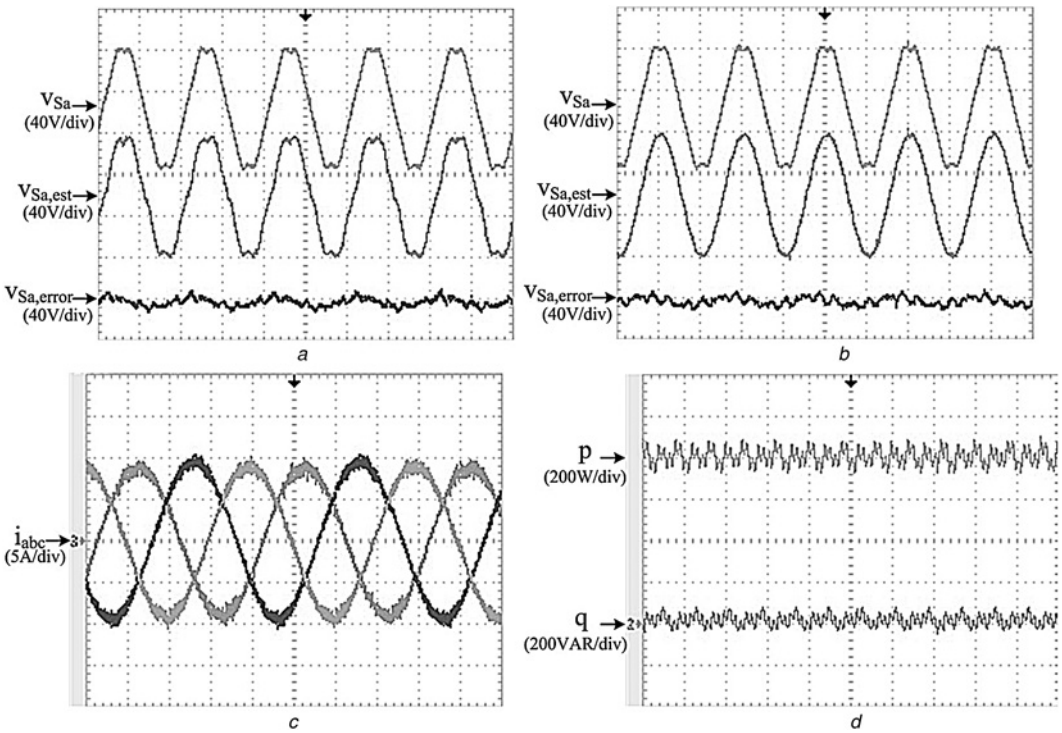

Fig. 7 *Experimental steady-state performance of the proposed grid voltage sensorless method*

a Actual grid voltage estimation with its harmonic contents
b Fundamental grid voltage estimation
c Three-phase grid currents
d Exchanged powers

doi: 10.1049/iet-pel.2014.0061

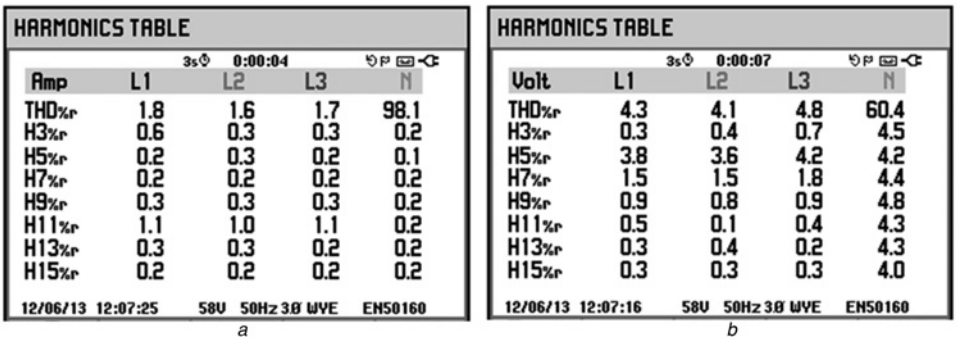

Fig. 8 *Experimental steady-state performance of the proposed grid voltage sensorless method*

a Grid current harmonics
b Grid voltage harmonics

investigations have been conducted on a 1 kVA VSC. The main parameters of the prototype VSC are summarised in Table 1, which are the same for both simulation and experimental tests. Simulation model has been established in MATLAB/SIMULINK and the schematic diagram of the experimental test bench is shown in Fig. 3. As depicted, the experimental setup includes a VSC, the TMS320F28335 digital signal controller (DSC), a digital to analogue (D/A) converter (AD7564), the Fluke 435 power quality analyser, power monitoring analogue board (composed of analogue multipliers AD633) to display the instantaneous powers. The DSC performs the proposed control scheme and sends waveforms of the estimated and measured grid voltages through the serial peripheral interface (SPI) to the AD7564 serial D/A converter. The D/A converts these digital data to analogue signals to be displayed on the oscilloscope.

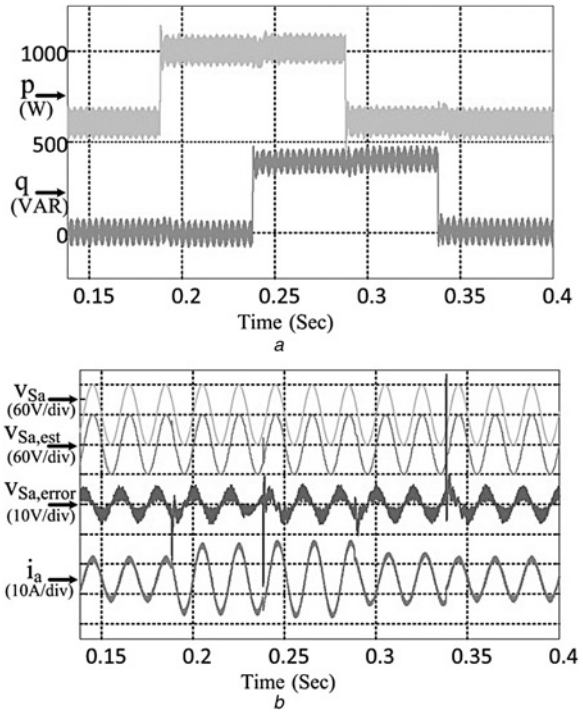

Fig. 9 *Simulated transient performance of the proposed method*

a Exchanged powers
b Transient waveforms

4.1 Startup performance

Figs. 4 and 5, respectively, show the simulated and experimental waveforms during the startup of the VSC. The grid voltage (v_{Sa}), the estimated voltage ($v_{Sa,\text{est}}$), the estimation error ($v_{Sa,\text{error}}$), and the grid current (i_a) are plotted in Figs. 4*a* and 5*a*. In addition, injected active and reactive powers into the grid and the number of iterations of the Newton–Raphson algorithm are shown in Figs. 4*b* and 5*b*, respectively. Clearly, the experimental waveforms are in good agreement with the simulation results.

As depicted in these figures, once the startup command is applied, that is, the reference current (power) jumps from zero to the desired value, the proposed estimation scheme

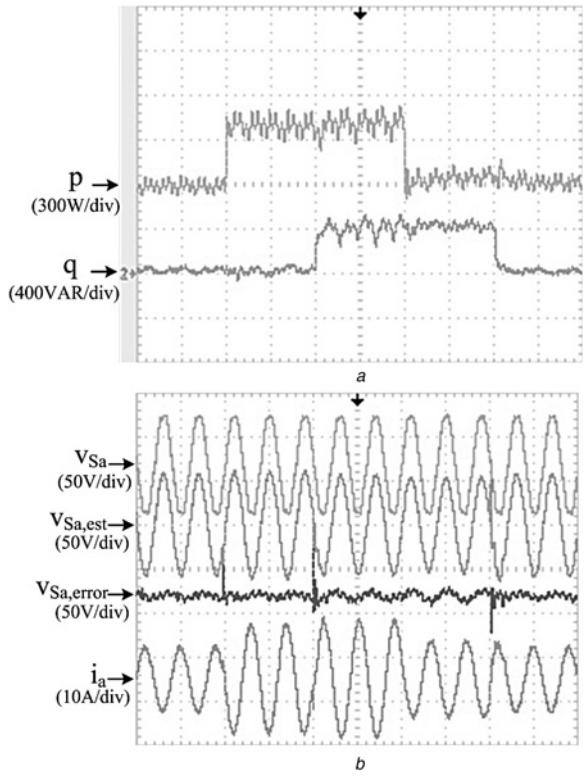

Fig. 10 *Experimental transient performance of the proposed method (time scale: 25 ms/div)*

a Exchanged powers
b Transient waveforms

can successfully rebuild the grid voltage estimated waveform within a few iterations (less than six iterations).

4.2 Steady-state performance

Simulation and experimental results of the proposed method in the steady-state operation are depicted in Figs. 6 and 7, respectively. Fig. 6 confirms the excellent performance of the proposed sensorless method under ideal grid voltage conditions, whereas Fig. 7 shows that in practical situations, even when the grid voltage is highly distorted, the control scheme can keep the injected currents to be sinusoidal and balanced. It is worth noting that if the input signal to the grid voltage estimator is selected as the sum of outputs of the PR-controller and the HC-network (v_{ref}), then the actual grid voltage with all its harmonic contents will be estimated (Fig. 7*a*). On the other hand, if only the output of PR-controller ($v_{ref,1}$) is used as the input signal to the estimator, the voltage estimator can successfully estimate the fundamental component of the distorted grid voltage (Fig. 7*b*). This attractive feature is derived from the intrinsic nature of the PR controller and harmonic compensator, because output of the resonator at any desired harmonic frequency has information of the grid voltage at that harmonic frequency. As shown in Fig. 1, in order to provide a sinusoidal template for the reference current generation, in our application, the fundamental component of the grid voltage is estimated and fed to the power estimator and the reference current calculator blocks.

The grid current harmonic spectrum under proposed control scheme is shown in Fig. 8*a*. As it can be seen, the THD is found to be 1.8% which meets the IEEE Std 519 recommendations.

4.3 Transient performance

Simulation and experimental results of the proposed method for several step changes in active and reactive powers are shown in Figs. 9 and 10, respectively. First, the reference value of active power is jumped from 600 to 1000 W and then is stepped back to 600 W, also the reference value of reactive power is step changed from 0 to 400 VAR and then to zero. The simulation and experimental results are in close with each other and confirm a fast and decoupled transient response to various step changes in the reference active and reactive powers. Also, Figs. 9*b* and 10*b* confirm that the voltage estimator offers a satisfactory performance at various step transients of the reference powers.

4.4 Robustness to filter impedance uncertainties

Fig. 11 shows the performance of the proposed estimation method with considering the mismatch in the filter impedance. The grid and estimated voltages and active and reactive powers are plotted in Fig. 11. The reference active and reactive powers are 800 W and 0 VAR, respectively. Clearly, for a wide range of parameter mismatches the grid voltage estimator can successfully generate the grid voltage fundamental component with minimum errors. This error

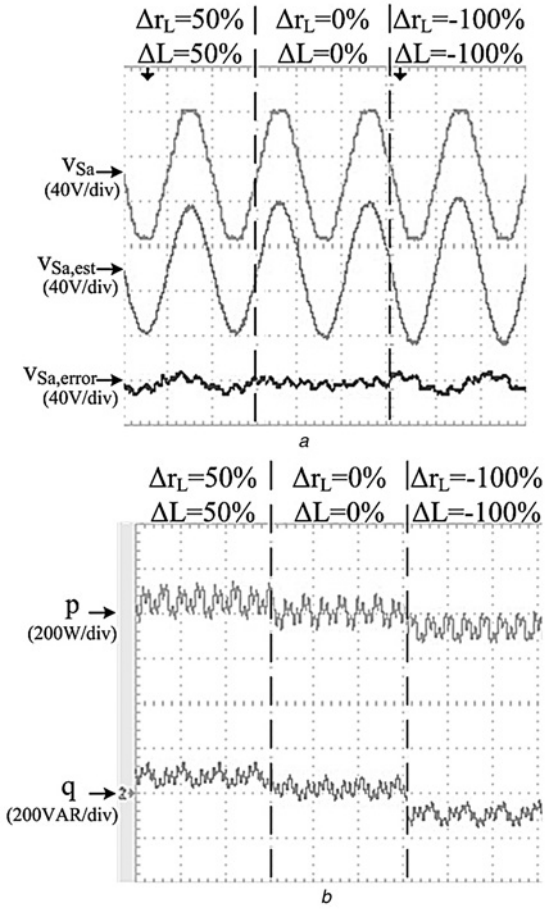

Fig. 11 *Experimental results showing the robustness of the proposed method to mismatch in the filter impedance*

a Converter waveforms
b Exchanged powers

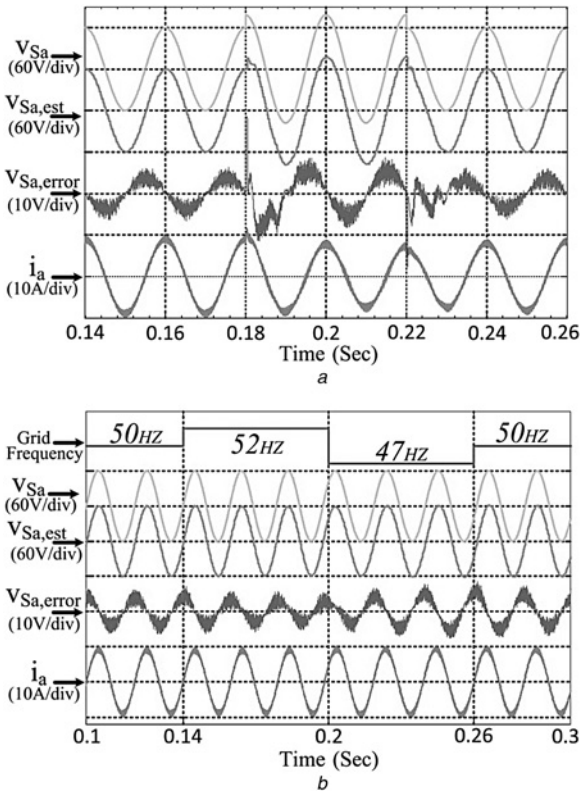

Fig. 12 *Simulated performance of the proposed method under grid disturbances*

a Grid amplitude changes
b Grid frequency changes

doi: 10.1049/iet-pel.2014.0061

appears as a small deviation in the output powers from their reference values. However, the system stability is not affected at all and a stable operation under all parameter mismatch conditions is achieved.

4.5 Performance under grid disturbances

Fig. 12*a* shows the performance of the proposed estimation scheme in response to step changes in the grid voltage amplitude, such that the grid voltage amplitude is increases by 30% at 0.18 s and then is decreased by 30% at 0.22 s. Also, proper operation of the proposed estimation scheme in the case of several step changes (up/down) in the grid voltage frequency is investigated and simulation results are depicted in Fig. 12*b*. Based on these figures, the grid voltage estimator can successfully estimate the grid voltage with minimum error despite of grid disturbances. Moreover, the system stability is not affected at all and a stable operation under both frequency and amplitude changes is achieved.

5 Conclusions

The possibility of replacing the grid voltage sensors with a voltage estimator scheme in the PR-based current control of the grid connected VSCs has been examined. The proposed voltage estimator employs the Newton–Raphson algorithm to solve the non-linear equations of the converter system. Moreover, by taking advantage of the PR controller, proposed voltage estimator can readily estimate the grid voltage fundamental component under distorted grid conditions.

The most important features of the proposed control method that are confirmed through experimental tests are:

- a simple structure and concept and ease of implementation;
- no need for coordinate transformations and a PLL;
- reduced cost, size and improved reliability of the system, which are consequences of eliminating the voltage sensors;
- full benefits of the PR current controller and harmonic compensators; and
- stable and acceptable operation in a wide range of parameter uncertainties, and grid voltage disturbances.

6 References

1 Yazdani, A., Iravani, R.: 'Voltage-sourced converters in power systems' (Wiley, 2010)
2 Teodorescu, R., Liserre, M., Rodriguez, P.: 'Grid converters for photovoltaic and wind power systems' (John Wiley & Sons, 2011)
3 Eloy-García1, J., Vasquez, J.C., Guerrero, J.M.: 'Grid simulator for power quality assessment of micro-grids', *IET Power Electron.*, 2013, **6**, (4), pp. 700–709
4 Xu, Y., Tolbert, L.M., Chiasson, J.N., Campbell, J.B., Peng, F.Z.: 'A generalised instantaneous non-active power theory for STATCOM', *IET Electr. Power Appl.*, 2007, **1**, (6), pp. 853–861
5 Mulla, M.A., Rajagopalan, C., Chowdhury, A.: 'Hardware implementation of series hybrid active power filter using a novel control strategy based on generalised instantaneous power theory', *IET Power Electron.*, 2013, **6**, (3), pp. 592–600
6 Cortés, P., Ortiz, P., Yuz, J.I., Rodríguez, J., Vazquez, S., Franquelo, L. G.: 'Model predictive control of an inverter with output *LC* Filter for UPS applications', *IEEE Trans. Ind. Electron.*, 2009, **56**, (6), pp. 1875–1883
7 Monfared, M., Sanatkar, M., Golestan, S.: 'Direct active and reactive power control of single-phase grid-tie converters', *IET Power Electron.*, 2012, **5**, (8), pp. 1544–1550
8 Jorge, S.G., Busada, C.A., Solsona, J.: 'Low computational burden grid voltage sensorless current controller', *IET Power Electron.*, 2013, **6**, (8), pp. 1592–1599
9 Noguchi, T., Tomiki, H., Kondo, S., Takahashi, I.: 'Direct power control of PWM converter without power-source Voltage sensors', *IEEE Trans. Ind. Appl.*, 1998, **34**, (3), pp. 473–479
10 Hansen, S., Malinowski, M., Blaabjerg, F., Kazmierkowski, M.P.: 'Sensorless control strategies for PWM rectifier'. Proc. Applied Power Electronics (APEC), New Orleans, 2000, vol. 2, pp. 832–838
11 Antoniewicz, P., Kazmierkowski, M.P.: 'Virtual flux based predictive direct power control of ac/dc converters with on-line inductance estimation', *IEEE Trans. Ind. Electron.*, 2008, **55**, (12), pp. 4381–4390
12 Malinowski, M., Jasinski, M., Kazmierkowski, M.P.: 'Simple direct power control of three-phase PWM rectifier using space-vector modulation (DPC-SVM)', *IEEE Trans. Ind. Electron.*, 2004, **51**, (2), pp. 447–454
13 Kulka, A.: 'Sensorless digital control of grid connected three phase converters for renewable sources'. Ph.D. dissertation, Norwegian Univ. Sci. Technol., Trondheim, Norway, 2009
14 Suul, J.A., Luna, A., Rodríguez, P., Undeland, T.: 'Voltage-sensor-less synchronization to unbalanced grids by frequency-adaptive virtual flux estimation', *IEEE Trans. Ind. Electron.*, 2012, **59**, (7), pp. 2910–2923
15 Hoffmann, N., Wilhelm, F.: 'Minimal invasive equivalent grid impedance estimation in inductive–resistive power networks using extended Kalman filter', *IEEE Trans. Power Electron.*, 2014, **29**, (2), pp. 631–641
16 Ahmed, K.H., Massoud, A.M., Finney, S.J., Williams, B.W.: 'Sensorless current control of three-phase inverter-based distributed generation', *IEEE Trans. Power. Deliv.*, 2009, **24**, (2), pp. 919–929
17 Leon, A.E., Solsona, J.A., Valla, M.I.: 'Control strategy for hardware simplification of voltage source converter-based power applications', *IET Power Electron.*, 2011, **4**, (1), pp. 39–50
18 Mohamed, Y.A.I., El-Saadany, E.F.: 'An Improved deadbeat current control scheme with a novel adaptive self-tuning load model for a three phase PWM voltage-source inverter', *IEEE Trans. Ind. Electron.*, 2007, **54**, (2), pp. 747–759
19 Mohamed, Y.A.I., Rahman, M.A., Seethapathy, R.: 'Robust line-voltage sensorless control and synchronization of *LCL*-filtered distributed generation inverters for high power quality grid connection', *IEEE Trans. Power Electron.*, 2012, **27**, (1), pp. 87–98
20 Mohamed, Y.A.I., El-Saadany, E.F.: 'Adaptive discrete-time grid-voltage sensorless interfacing scheme for grid-connected DG-inverters based on neural network identification and deadbeat current regulation', *IEEE Trans. Power Electron.*, 2008, **23**, (1), pp. 308–321
21 Mohamed, Y.A.I., El-Saadany, E.F.: 'A robust natural-frame-based interfacing scheme for grid-connected distributed generation inverters', *IEEE Trans. Energy Convers.*, 2011, **26**, (3), pp. 728–736
22 Wei, Z., Chen, J., Chen, X., Gong, C., Fan, Y.: 'Modified one-cycle-controlled three-phase pulse-width modulation rectifiers under low-output', *IET Power Electron.*, 2014, **7**, (3), pp. 753–763
23 Chongming, Q., Smedley, K.M.: 'Unified constant-frequency integration control of three-phase standard bridge boost rectifiers with power-factor correction', *IEEE Trans. Ind. Electron.*, 2003, **50**, (1), pp. 100–107
24 Ghodke, A., Chatterjee, K.: 'One-cycle-controlled bidirectional three-phase unity power factor ac–dc converter without having voltage sensors', *IET Power Electron.*, 2012, **5**, (9), pp. 1944–1955
25 Dai, M., Marwali, M.N., Jung, J.W., Keyhani, A.: 'Power flow control of a single distributed generation unit', *IEEE Trans. Power Electron.*, 2008, **23**, (1), pp. 322–331
26 Blaabjerg, F., Teodorescu, R., Liserre, M., Timbus, A.V.: 'Overview of control and grid synchronization for distributed power generation systems', *IEEE Trans. Ind. Electron.*, 2006, **53**, (5), pp. 1398–1409
27 Castilla, M., Miret, J., Matas, J., de Vicuña, L.G., Guerrero, J.M.: 'Control design guidelines for single-phase grid-connected photovoltaic inverters with damped resonant harmonic compensators', *IEEE Trans. Ind. Electron.*, 2009, **56**, (11), pp. 4492–4501
28 Vidal, A., Freijedo, F.D., Yepes, A.G., *et al.*: 'Assessment and optimization of the transient response of proportional-resonant current controllers for distributed power generation systems', *IEEE Trans. Power Electron.*, 2013, **60**, (4), pp. 1367–1383
29 Yepes, A., Freijedo, F., Doval-Gandoy, J., Lopez, O., Malvar, J., Fernandez-Comesana, P.: 'Effects of discretization methods on the performance of resonant controllers', *IEEE Trans. Power Electron.*, 2010, **25**, (7), pp. 1692–1712
30 Vasquez, J.C., Guerrero, J.M., Luna, A., Rodriguez, P., Teodorescu, R.: 'Adaptive droop control applied to voltage-source inverters operating in grid-connected and islanded modes', *IEEE Trans Ind. Electron.*, 2009, **56**, (10), pp. 4088–4096
31 De Brabandere, K., Bolsens, B., Van den Keybus, J., Woyte, A., Driesen, J., Belmans, A.: 'A voltage and frequency droop control method for parallel inverters', *IEEE Trans. Power Electron.*, 2007, **22**, (4), pp. 1107–1115